Proceeding of the IEEE
International Conference on Robotics and Biomimetics
Dali, China, December 2019

Walking of Biped Robot with Variable Stiffness at the Ankle Joint*

Qing Bi[1], Yixiang Liu[2], Xizhe Zang[3], Rui Song[2], Haibin Wang[1], and Weimin Li[1]

1. Shandong Institute of Advanced Technology, Chinese Academy of Sciences, Jinan 250001, China
2. School of Control Science and Engineering, Shandong University, Jinan 250061, China
3. State Key Laboratory of Robotics and System, Harbin Institute of Technology, Harbin 150080, China

biqing_meng@126.com, liuyixiang@sdu.edu.cn, zangxizhe@hit.edu.cn,
rsong@sdu.edu.cn, hb.wang@sdiat.ac.cn, wm.li@sdiat.ac.cn

***Abstract* - Achieving versatile and efficient walking on biped robots is an important research objective. The impact between the foot and the ground has significant effects on the walking stability of biped robots. Research on human walking indicates that the joints in human lower limbs show different stiffness values in different phases of walking. Inspired by humans, this paper presents the realization of biped robot walking with variable stiffness at the ankle joint. A walking control scheme which combines PD control and variable impedance control is designed for the biped robot. Results of dynamic walking simulation verified that variable stiffness at the ankle joint could contribute to the improvement of walking stability and energy efficiency.**

Index Terms - Biped robot, walking control, variable stiffness, impedance control.

I. Introduction

Owing to high mobility, biped robots can replace or assist humans in performing various high-risk and high-intensity tasks in complex environments, for instance, search and rescue [1, 2], firefighting [3], and other disaster response scenarios [4]. Having similar appearance with humans, biped robots are more adaptable for applications in our daily life [5-7]. As a typical unstable system, the walking stability of biped robot is always the research priority. During walking of biped robot, although the impact between the foot and the ground takes a short time, it has significant effect on the walking stability. At the moment of foot-ground contact, the impulse force from the ground causes sudden changes in the velocity of the biped robot. If the changes of robot motion exceed the margin of stability, the biped robot system becomes unstable. Consequently, the joint actuators will adjust the posture of the biped robot based on the caused changes in order to keep its stability under the control system, which results in extra energy consumption.

Another important feature of biped robot walking is that the contact between the foot and the ground is in a unilateral constraint state. For many biped robots, materials with a high coefficient of friction are added to the soles to avoid sliding of the foot. However, when the impact happens, the foot that contacts with the ground will rebound and vibrate due to the impulse forces, causing deviation between the actual landing point and the planned landing point of the foot. This may lead to the foot stepping empty and the biped robot falling down. In addition, excessive impact forces will even damage the motors, reducers and other precision components in the transmission system of the biped robot [8].

For the above reasons, reducing the landing impact has always been an important research topic in the field of biped robots. On one hand, some researchers focused on the modelling of foot-ground contact process, and verified the proposed models through simulation or experiments [9-11]. On the other hand, the effects of foot-ground impact on the biped robot system including structure design, gait planning and walking control strategy were studied so as to reduce the impact forces. According to relevant studies, the impact and vibration of the landing on the biped robot can be effectively reduced by adding compliance materials and mechanisms on the foot sole [12]. Considering that the ankle joint which connects the foot and shank is the nearest joint from the ground, variable stiffness at the ankle joint will be beneficial for improving the walking stability of biped robots.

The objective of this paper is to realize walking of biped robot with variable stiffness at the ankle joint by mimicking human walking mechanisms. The rest of this paper is organized as follows. Section II introduces analysis about the stiffness of human ankle joint. Section III presents the control scheme of the biped robot for walking with variable stiffness at the ankle joint. Results of dynamic walking simulation are presented in Section IV. Finally, some conclusions of this study are given in Section V.

II. Stiffness of Human Ankle Joint

A. Human Walking Simulation

In different phases of human walking, leg muscles perform rhythmic contraction and relaxation, so that they show different levels of muscle strength. For example, when the leg moves forward, the muscles contract to make the foot of the swing leg move quickly and accurately to the desired

* This work is supported by the National Natural Science Foundation of China under Grant 51675116 and the National Key Research and Development Plan of China under Grant 2017YFC0806501.
Corresponding author: Yixiang Liu.

978-1-7281-6321-5/19//$31.00 ©2019 IEEE

position. When the foot of the swing leg touches the ground, the leg muscles expand to cushion the impact between the foot and the ground, ensuring the smoothness and stability of the touching process.

In order to estimate the stiffness of human ankle joint, human walking simulation is carried out in the software OpenSim. OpenSim is an open-source platform for modeling, simulation, and analysis of neuro-musculoskeletal systems [13]. In OpenSim, human body is represented by a musculoskeletal model with 23 degrees-of-freedom (DOF) which is actuated by 54 musculotendon actuators. The hip is modeled as a 3-DOF ball-and-socket joint, and the knee and ankle joints are all modeled as 1-DOF revolute joints [14].

To simulate human walking, the experimental data including trajectories of markers on the body and ground reaction forces and moments was collected while a subject was walking. Then a set of muscle excitations was computed which was required to closely track the kinematics generated by solving an optimization problem [15]. Fig. 1 shows the snapshots of the obtained subject-specific walking simulation in OpenSim. After simulation, the kinematics and kinetics of the human body during walking can be obtained.

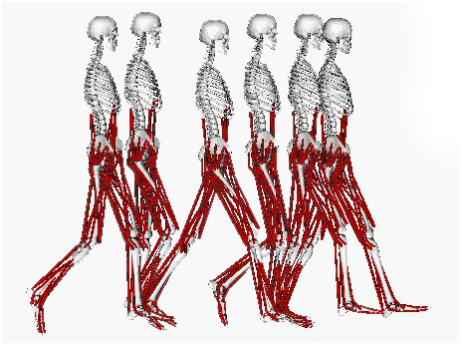

Fig. 1 Snapshots of simulated human walking in OpenSim.

B. *Quasi-stiffness of Human Ankle Joint*

Joint stiffness can be derived from muscle and tendon forces, tendon strains, and moment arms of each muscle with respect to each joint. But it is difficult to obtain joint stiffness. In this paper, a relatively simple method is adopted to estimate the equivalent stiffness of the joint, that is, the joint is regarded as a whole, without considering the driving mode and structural composition of the joint, but solving the joint stiffness according to the changing relationship between the input, i.e. driving torque and output, i.e. rotation angle of the joint. In other words, the joint stiffness is expressed as the finite difference between joint torque and joint angle. The obtained joint stiffness is termed as quasi-stiffness.

The torque-angle relation curve and joint quasi-stiffness of the ankle joint are given in Fig. 2 and Fig. 3 respectively. As can be seen from the figure, the ankle joint curve is composed of a counterclockwise closed ring, and the whole curve can be roughly divided into four stages, i.e., AB, BC, CD and DE. AB segment corresponds to the first half of the prophase of support, and the ankle produces a slight metatarsal flexion. The BC segment corresponds to the posterior half of the prophase and the middle stage of the prophase. CD segment corresponds to the later support period and the earlier swing period. The DA segment corresponds to the middle and late stage of swing, when the ankle joint performs dorsiflexion and returns to the neutral position. By linear fitting for each stage, the joint stiffness of each stage can be obtained. Except for the slightly poor linearity of BC segment, the linearity of other segments is higher. The analysis indicates that the ankle joint shows three stiffness values during the whole gait cycle of walking.

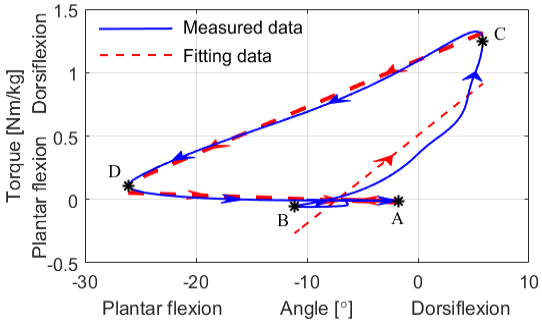

Fig. 2 The torque-angle relation curve of the ankle joint.

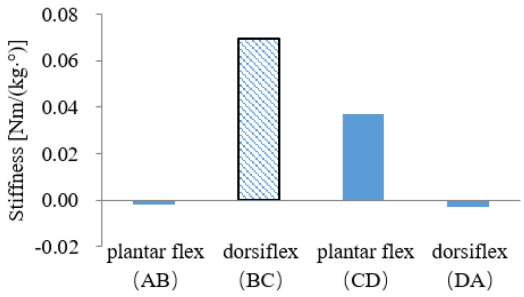

Fig. 3 Quasi-stiffness of the ankle joint.

III. Biped Robot Walking with Variable Stiffness

A. *The Gait of Biped Robot*

The gait of the biped robot is designed based on human walking. A complete gait cycle includes single support phase and double support phase, as shown in Fig. 4. The gait cycle starts at toe-off of one foot and ends at subsequent toe-off of the same foot. In double support phase, both the two feet rotate relative to the ground, enabling the center of pressure of the biped robot on the ground to make a smooth transition from the original support foot to the new support foot.

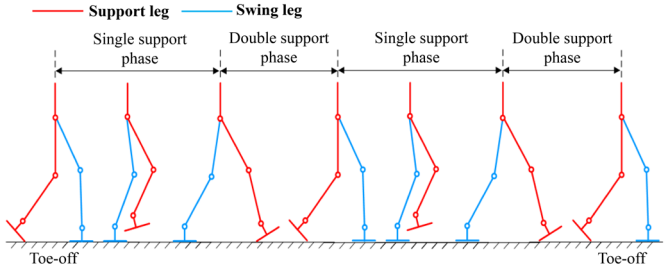

Fig. 4 A gait cycle of the biped robot.

The trajectories of each joint in a gait cycle can be obtained through off-line gait planning. In single support phase, the trajectory planning of the hip joint is based on the

linear inverted pendulum model [16]. In double support phase, the biped robot needs to switch the support leg. The linear inverted pendulum model is no longer applicable. Thus, the trajectory planning of the hip joint in this phase is realized through polynomial interpolation. The trajectory of ankle joint is planned using three-points interpolation method. Taking the initial point, the highest point and end point of the ankle joint in single support phase as interpolation points and the velocity of the initial point and the end point as boundary conditions, the corresponding cubic spline curve can be calculated, as shown in Fig. 5. Then the trajectory of the knee joint can be derived from inverse kinematics based on the trajectories of the hip and knee joints. After all the joint trajectories were determined, the changes of posture of the biped robot in a complete gait cycle can be visualized in Fig. 6.

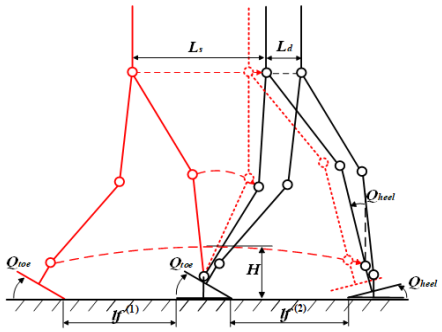

Fig. 5 Trajectory planning of the ankle joint.

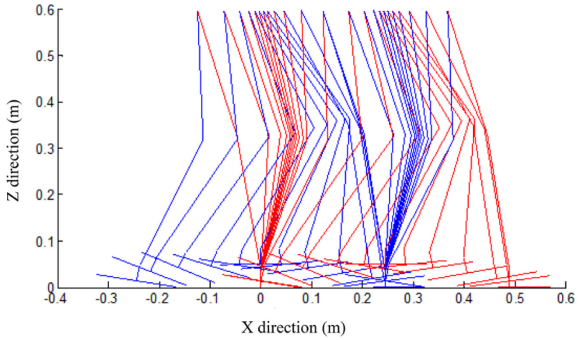

Fig. 6 The planned gait of the biped robot.

B. *Walking Control of the Biped Robot*

Inspired by the human walking control strategy, a composite controller which combines PD control and variable impedance control is proposed in this study, as presented in Fig. 7. The PD controller is used for fast tracking control of the desired trajectory of the biped robot, while the variable impedance controller is used at the joint layer for adjusting the stiffness parameters of the ankle joints timely and making the biped robot exhibit the desired compliance. In more detail, when the leg swings forward, the PD controller plays a major role, and the variable impedance controller plays a secondary role to compensate the tracking error caused by the nonlinear dynamics model of the biped robot. When the biped robot is about to make foot-ground contact, the variable impedance controller lowers the stiffness and increases the damping of the ankle joint in advance to absorb the impact and prevent the driver producing negative work, which improves the stability and efficiency of the system.

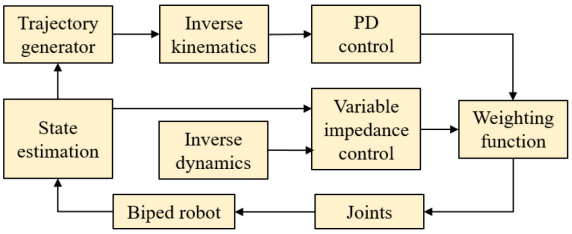

Fig. 7 Walking control scheme of the biped robot.

The composite controller has the following form:

$$\tau_j = w_1\tau_{PD}\left(\theta_a,\theta_d,\dot{\theta}_a,\dot{\theta}_d,K_p,K_d\right)+w_2\tau_{im}\left(\theta,\dot{\theta},k,b\right)$$

where w_1 and w_2 are the weighting coefficients of PD controller and variable impedance controller, and w_1+w_2=1. The values of the coefficients are determined by the state and phase of walking.

The control output of PD controller is obtained from the desired joint trajectory of the biped robot:

$$\tau_{PD} = K_p\left(\theta_a-\theta_d\right)+K_d\left(\dot{\theta}_a-\dot{\theta}_d\right)$$

where K_p and K_d are proportional coefficient matrix and differential coefficient matrix respectively.

The control output of the variable impedance controller can be written as:

$$\tau_{\text{im}} = k_j\left(\theta-\theta^e\right)+b_j\dot{\theta}$$

where k_j and b_j represent the stiffness coefficient and damping coefficient of the ankle joint respectively.

IV. Simulation and Verification

A. *Dynamic Walking Simulation of the Biped Robot*

In order to verify the gait planning and control strategy of the biped robot, a simplified virtual model of biped robot was established. The biped robot model is composed of seven parts, i.e., the trunk, thighs, shanks, and feet, which are connected by the hip, knee, and ankle joints respectively. The continuous walking process of the biped robot was co-simulated using Adams and Matlab, as shown in Fig. 8. For comparison, two simulation conditions were set up, namely, rigid ankle joints and variable stiffness ankle joints. After the completion of the dynamic walking simulation, the results were analyzed from three aspects, namely, the contact forces between the foot and the ground, joint energy consumption and ZMP trajectory.

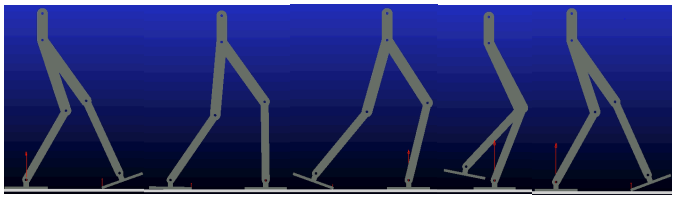

Fig. 8 Dynamic walking simulation of the biped robot.

B. *Contact Forces*

In the walking simulation under the condition of rigid ankle joint, the force between the feet and ground is shown in Fig. 9(a). As can be seen from the figure, there is a significant sudden change in the forces at the moment of the impact. Taking the left leg as an example, at the moment of heel

contact, the left foot received a ground impact of about 37N. At the same time, the force between the right foot and the ground dropped from 148N to 99N. At the subsequent point of toe contact, the force between left foot and ground increased from 24N to 121N, and the force between right foot and ground decreased by the same amount at that moment. Under the current planned gait, the transition between the swing foot and the support foot is extremely unstable, and the impact of toe contact is far greater than that of heel contact.

In the walking simulation under the condition of variable stiffness ankle joint, the force between the feet and the ground is shown in Fig. 9(b). Compared with Fig. 9(a), the sudden change of foot and ground forces decreased significantly. Taking the left leg as an example, at the time of heel contact, the left foot received ground impact force of about 20N, and the right foot received no significant change in force at the same time. From heel contact to toe contact, the force between the contact foot and the ground increased steadily, while the force between the original support foot and the ground decreased steadily. According to the contact force curve shown in the figure, there was no significant sudden change in the contact force at the moment of toe contact, which proved that the variable stiffness ankle joint could effectively buffer the impact between the foot and the ground, and realize smooth switch between the swing foot and the support foot in double support phase.

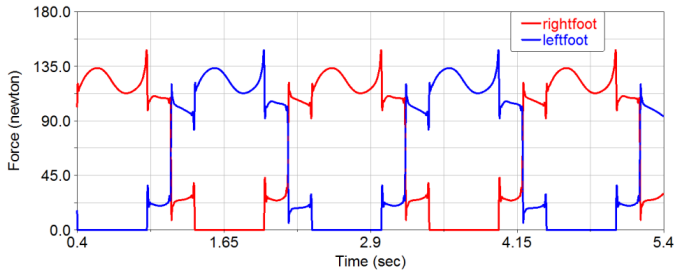

(a) The biped robot walking with rigid ankle joint.

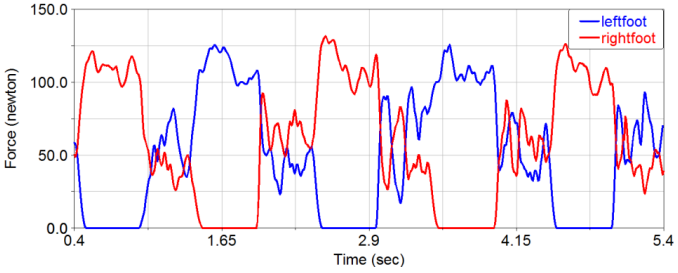

(b) The biped robot walking with variable stiffness ankle joint.

Fig. 9 Comparisons of contact forces of the biped robot.

C. *Joint Power*

When analyzing the joint power of two walking simulations, the joint power of ankle, knee and hip joints within a walking cycle measured by Adams software was filtered by a butterworth low-pass filter at a cut-off frequency of 0.01Hz. Fig. 10 shows the comparisons of joint power between the two conditions. It can be found that the presence of variable stiffness ankle joint reduces the peak power of the hip, knee and ankle joint in a gait cycle. Among them, the peak power of the hip joint and knee joint located in the swing leg decreased significantly during foot-ground contact, while the power of the ankle joint of the swing leg did not show significant decrease during the same period.

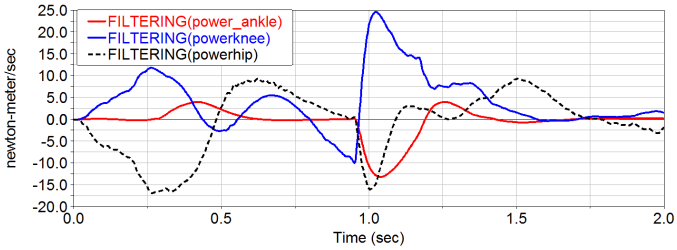

(a) The biped robot walking with rigid ankle joint.

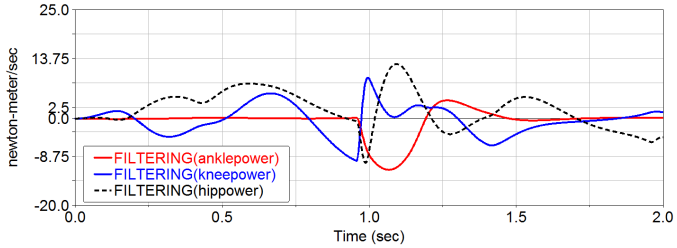

(b) The biped robot walking with variable stiffness ankle joint.

Fig. 10 Comparisons of joint power of the biped robot.

D. *ZMP Trajectory*

Fig. 11 presents the comparisons of ZMP trajectories between the two walking conditions. From this figure, it can be found that the variable stiffness ankle joint greatly improves the smoothness of ZMP trajectories. Compared with walking with rigid ankle joint, the ZMP trajectory of the biped robot with variable stiffness ankle joint could track the planned ZMP better. Thus, the variable stiffness at the ankle joint could help improve walking stability.

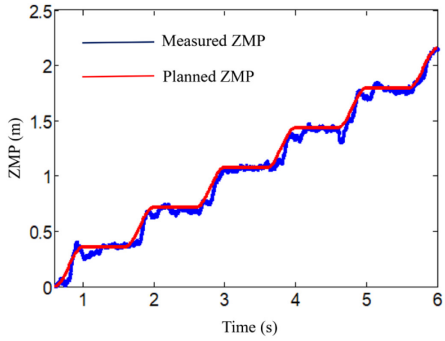

(a) ZMP trajectories of walking with rigid ankle joint.

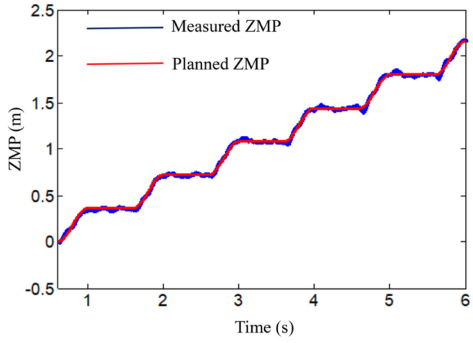

(b) ZMP trajectories of walking with variable stiffness ankle joint.

Fig. 11 Comparisons of ZMP trajectories of the biped robot.

V. CONCLUSION

In this paper, the stiffness of human ankle joint during walking is analyzed through simulation, which indicates that the ankle joint shows different stiffness in different walking phases. On this basis, a walking gait with variable stiffness at the ankle joint is proposed for biped robot. A walking control scheme combining PD control and variable impedance control is designed for the biped robot. Dynamic walking simulation verified that variable stiffness at the ankle joint could help to increase walking stability and energy efficiency. In the future, we will expand the feature of variable stiffness to all joints of the biped robot, and study its walking control scheme.

ACKNOWLEDGMENT

The work reported in this paper is supported by the National Natural Science Foundation of China under Grant 51675116 and the National Key Research and Development Plan of China under Grant 2017YFC0806501.

REFERENCES

[1] R. O'Flaherty, P. Vieira, M. X. Grey, P. Oh, and M. Stilman, "Humanoid robot teleoperation for tasks with power tools," in *Proceedings of the 2013 IEEE Conference on Technologies for Practical Robot Applications*, Woburn, MA, USA, 2013, pp. 1-6.

[2] S. Hong, G. Park, Y. Lee, W. Lee, B. Choi, and O. Sim, et al, "Development of a tele-operated rescue robot for a disaster response," *International Journal of Humanoid Robotics*, vol. 15, no. 4, 2018, pp. 1850008.

[3] A. Wagoner, A. Jagadish, E. T. Matson, E. Lee, Y. Nah, and K. Tae, et al, "Humanoid robots rescuing humans and extinguishing fires for Cooperative Fire Security System using HARMS," in *Proceedings of the 2015 6th International Conference on Automation, Robotics and Applications*, Queenstown, New Zealand, 2015, pp. 411-415.

[4] H. Dang, Y. Jun, P. Oh, and P. K. Allen, "Planning Complex Physical Tasks for Disaster Response with a Humanoid Robot," in *Proceedings of the 2013 IEEE International Conference on Technologies for Practical Robot Applications*, Woburn, MA, USA, 2013, pp. 1-6.

[5] Y. Sakagami, R. Watanabe, C. Aoyama, S. Matsunaga, N. Higaki, and K. Fujimura, "The intelligent ASIMO: system overview and integration," in *Proceedings of the 2002 IEEE/RSJ International Conference on Intelligent Robots and System*, Lausanne, Switzerland, 2002, pp. 2478-2483.

[6] K. Kaneko, F. Kanehiro, M. Morisawa, T. Tsuji, K. Miura, and S. Nakaoka, et al, "Hardware improvement of cybernetic human hrp-4c for entertainment use," in *Proceedings of the 2011 IEEE/RSJ International Conference on Intelligent Robots and Systems*, San Francisco, CA, USA, 2011, pp. 4392-4399.

[7] S. Nugroho, A. Prihatmanto, and A. Rohman, "Design and implementation of kinematics model and trajectory planning for NAO humanoid robot in a tic-tac-toe board game," in *Proceedings of the 2014 IEEE 4th International Conference on System Engineering and Technology*, Bandung, Indonesia, 2014, pp. 1-7.

[8] Y. Liu, X. Zang, Z. Lin, and J. Zhao, "Concept and Design of a Lightweight Biped Robot for Walking on Rough Terrain," in *Proceedings of the 2017 IEEE International Conference on Robotics and Biomimetics*, Macau, China, 2017, pp. 1240-1245.

[9] L. Ding, H. Gao, Z. Deng, J. Song, Y. Liu, and G. Liu, et al, "Foot-terrain interaction mechanics for legged robots: modeling and experimental validation," *The International Journal of Robotics Research*, vol. 32, no. 13, 2013, pp. 1585-1606.

[10] Q. Wang, K. Wei, L. Wang, and D. Lv, "Modeling and stability analysis of human normal walking with implications for the evolution of the foot," in *Proceedings of the 2010 3rd IEEE RAS & EMBS International Conference on Biomedical Robotics and Biomechatronics*, Tokyo, Japan 2010, pp. 479-484.

[11] R. Pàmies-Vilà, J. M. Font-Llagunes, U. Lugrís, and J. Cuadrado, "Parameter identification method for a three-dimensional foot-ground contact model," *Mechanism and Machine Theory*, vol. 75, no. 5, 2014, pp. 107-116.

[12] A. Najmuddin, Y. Fukuoka, and S. Ochiai, "Experimental development of stiffness adjustable foot sole for use by bipedal robots walking on uneven terrain," in *Proceedings of the 2012 IEEE/SICE International Symposium on System Integration*, Fukuoka, Japan, 2012, pp. 248-253.

[13] R. Bortoletto, E. Pagello, and D. Piovesan, "Effects of reserve actuators on optimization solutions: From muscle force to joint stiffness," in *Proceedings of the 2015 IEEE International Conference on Rehabilitation Robotics*, Singapore, 2015, pp. 973-978.

[14] Y. Liu, X. Zang, C. Wang, and Y. Liu, "A Bio-Inspired Musculoskeletal Model of the Lower Limb for Energy Economical Bipedal Walking," in *Proceedings of the 2019 Third IEEE International Conference on Robotic Computing*, Naples, Italy, 2019, pp. 288-292.

[15] D. G. Thelen, and F. C. Anderson, "Using computed muscle control to generate forward dynamic simulations of human walking from experimental data," *Journal of Biomechanics*, vol. 39, no. 6, 2006, pp. 1107-1115.

[16] S. Kajita, F. Kanehiro, K. Kaneko, K. Yokoi, and H. Hirukawa, "The 3D linear inverted pendulum mode: a simple modeling for a biped walking pattern generation," in *Proceedings of the 2001 IEEE/RSJ International Conference on Intelligent Robots and Systems*, Maui, Hawaii, USA, 2001, pp. 239-246.